INVARIANT MANIFOLDS, THE SPATIAL THREE-BODY PROBLEM AND SPACE MISSION DESIGN

G. Gómez[*], W.S. Koon[†], M.W. Lo[‡],
J.E. Marsden[§], J. Masdemont[¶], and S.D. Ross[‖]

The invariant manifold structures of the collinear libration points for the spatial restricted three-body problem provide the framework for understanding complex dynamical phenomena from a geometric point of view. In particular, the stable and unstable invariant manifold "tubes" associated to libration point orbits are the phase space structures that provide a conduit for orbits between primary bodies for separate three-body systems. These invariant manifold tubes can be used to construct new spacecraft trajectories, such as a "Petit Grand Tour" of the moons of Jupiter. Previous work focused on the planar circular restricted three-body problem. The current work extends the results to the spatial case.

INTRODUCTION

New space missions are increasingly more complex. They require new and unusual kinds of orbits to meet their scientific goals, orbits which cannot be found by the traditional conic approach. The delicate heteroclinic dynamics employed by the *Genesis Discovery Mission* dramatically illustrates the need for a new paradigm: study of the three-body problem using dynamical systems theory.[1,2,3]

Furthermore, it appears that the dynamical structures of the three-body problem (e.g., stable and unstable manifolds, bounding surfaces), reveal much about the morphology and transport of materials within the solar system. The cross-fertilization between the study of the natural dynamics in the solar system and applications to engineering has produced a number of new techniques for constructing spacecraft trajectories with desired behaviors, such as rapid transition between the interior and exterior Hill's regions, temporary capture, and collision.[4]

The invariant manifold structures associated to the collinear libration points for the restricted three-body problem, which exist for a range of energies, provide a framework for understanding

[*]Departament de Matemàtica Aplicada i Anàlisi, Universitat de Barcelona, Barcelona, Spain. Email: gomez@cerber.mat.ub.es

[†]Control and Dynamical Systems, California Institute of Technology, MC 107-81, Pasadena, California 91125, USA. Email: koon@cds.caltech.edu

[‡]Navigation and Mission Design Section, Jet Propulsion Laboratory, California Institute of Technology, Pasadena, CA 91109, USA. Email: Martin.Lo@jpl.nasa.gov

[§]Control and Dynamical Systems, California Institute of Technology, MC 107-81, Pasadena, California 91125, USA. Email: marsden@cds.caltech.edu

[¶]Departament de Matemàtica Aplicada I, Universitat Politècnica de Catalunya, Barcelona, Spain. Email: josep@barquins.upc.es

[‖]Control and Dynamical Systems, California Institute of Technology, MC 107-81, Pasadena, California 91125, USA. Email: shane@cds.caltech.edu

these dynamical phenomena from a geometric point of view. In particular, the stable and unstable invariant manifold tubes associated to libration point orbits are the phase space structures that provides a conduit for material to and from the smaller primary body (e.g., Jupiter in the Sun-Jupiter-comet three-body system), and between primary bodies for separate three-body systems (e.g., Saturn and Jupiter in the Sun-Saturn-comet and the Sun-Jupiter-comet three-body systems).[5]

Furthermore, these invariant manifold tubes can be used to produce new techniques for constructing spacecraft trajectories with interesting characteristics. These may include mission concepts such as a low energy transfer from the Earth to the Moon and a "Petit Grand Tour" of the moons of Jupiter. See Figures 1 and 2. Using the invariant manifold structures of the 3-body systems, we were able to construct a transfer trajectory from the Earth which executes an unpropelled (i.e., ballistic) capture at the Moon.[6] An Earth-to-Moon trajectory of this type, which utilizes the perturbation by the Sun, requires less fuel than the usual Hohmann transfer.
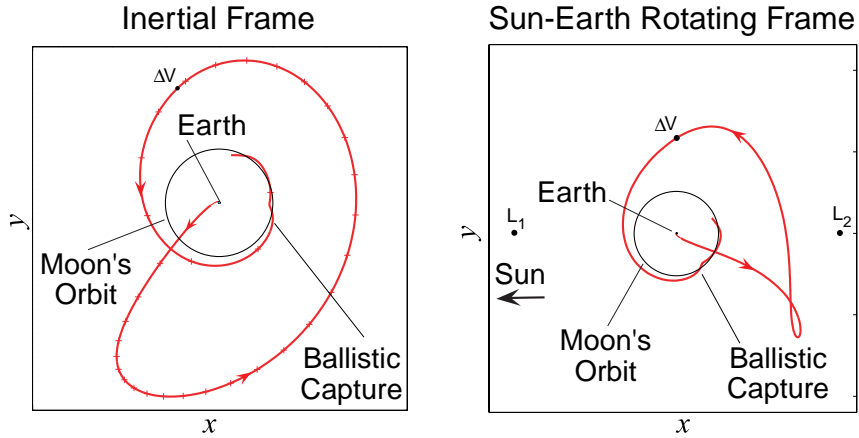

Figure 1: (a) Low energy transfer trajectory in the geocentric inertial frame. (c) Same trajectory in the Sun-Earth rotating frame.
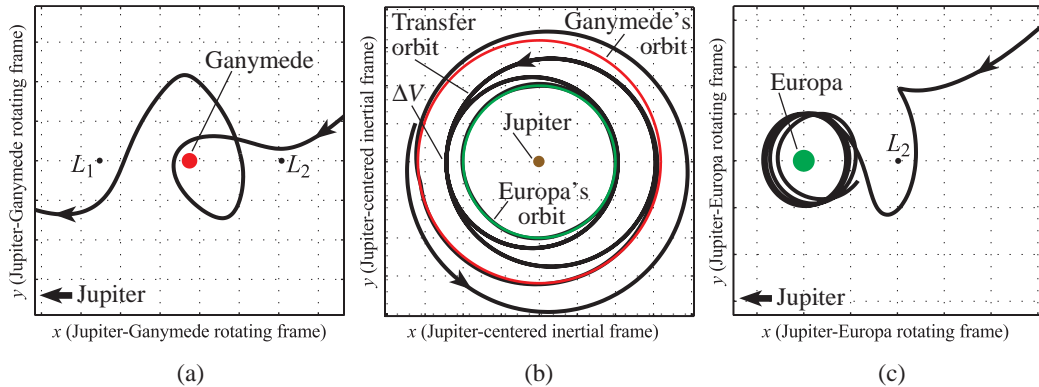

Figure 2: The "Petit Grand Tour" space mission concept for the Jovian moons. In our previous study, we showed an orbit coming into the Jupiter system and (a) performing one loop around Ganymede (shown in the Jupiter-Ganymede rotating frame), (b) transferring from Ganymede to Europa using a single impulsive maneuver (shown in the Jupiter-centered inertial frame), and (c) getting captured by Europa (shown in the Jupiter-Europa rotating frame).

2

Moreover, by decoupling the Jovian moon n-body system into several three-body systems, we can design an orbit which follows a prescribed itinerary in its visit to Jupiter's many moons. In an earlier study of a transfer from Ganymede to Europa,[7] we found our transfer ΔV to be half the Hohmann transfer value. As an example, we generated a tour of the Jovian moons: starting beyond Ganymede's orbit, the spacecraft is ballistically captured by Ganymede, orbits it once and escapes, and ends in a ballistic capture at Europa. One advantage of this Petit Grand Tour as compared with the Voyager-type flybys is the "leap-frogging" strategy. In this new approach to space mission design, the spacecraft can circle a moon in a loose temporary capture orbit for a desired number of orbits, perform a transfer ΔV and become ballistically captured by another adjacent moon for some number of orbits, etc. Instead of flybys lasting only seconds, a scientific spacecraft can orbit several different moons for any desired duration.

The design of the Petit Grand Tour in the planar case is guided by two main ideas. First, the Jupiter-Ganymede-Europa-spacecraft four-body system is approximated as two coupled planar three-body systems. Then, the invariant manifold tubes of the two planar three-body systems are used to construct an orbit with the desired behaviors. This initial solution is then refined to obtain a trajectory in a more accurate 4-body model. See Figure 3.
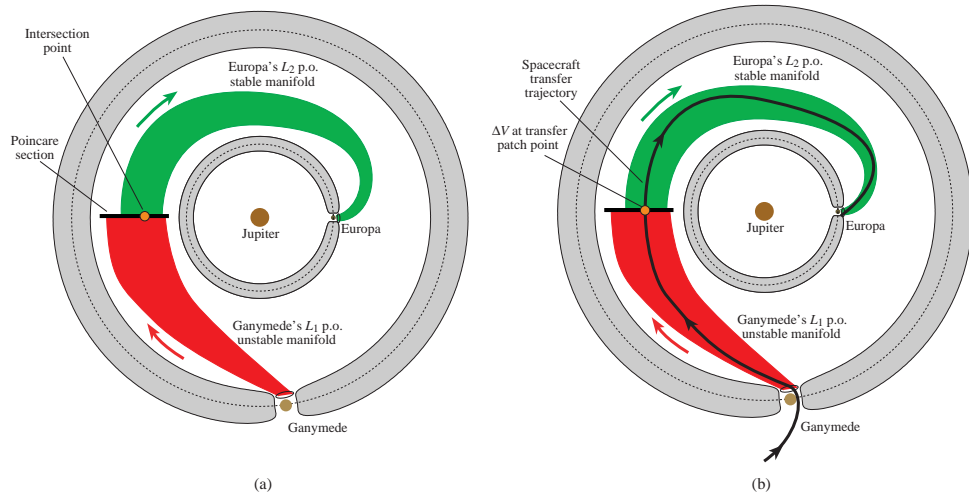

Figure 3: (a) Find an intersection between dynamical channel enclosed by Ganymede's L_1 periodic orbit unstable manifold and dynamical channel enclosed by Europa's L_2 periodic orbit stable manifold (shown in schematic). (b) Integrate forward and backward from patch point (with ΔV to take into account velocity discontinuity) to generate desired transfer between the moons (schematic).

The **coupled 3-body model** considers the two adjacent moons competing for control of the same spacecraft as two nested 3-body systems (e.g., Jupiter-Ganymede-spacecraft and Jupiter-Europa-spacecraft). When close to the orbit of one of the moons, the spacecraft's motion is dominated by the 3-body dynamics of the corresponding planet-moon system. Between the two moons, the spacecraft's motion is mostly planet-centered Keplerian, but is precariously poised between two competing 3-body dynamics. In this region, orbits connecting unstable libration point orbits of the two different 3-body systems may exist, leading to complicated transfer dynamics between the two adjacent moons. We seek intersections between invariant manifold tubes which connect the capture regions around each moon. In the planar case, these tubes separate transit orbits (inside the tube) from non-transit orbits (outside the tube). They are the phase space structures that provide a conduit for orbits between regions within each three-body systems as well as between primary bodies for separate three-body systems.[4] The extension of this planar result to the spatial case is the subject of the current paper.

Extending Results from Planar Model to Spatial Model Previous work based on the planar circular restricted three-body problem (PCR3BP) revealed the basic structures controlling the dynamics.[4,5,6,7] But future missions will require three-dimensional capabilities, such as control of the latitude and longitude of a spacecraft's escape from and entry into a planet or moon. For example, the proposed Europa Orbiter mission desires a capture into a high inclination polar orbit around Europa. Three-dimensional capability is also required when decomposing an n-body system into three-body systems that are not co-planar, such as the Earth-Sun-spacecraft and Earth-Moon-spacecraft systems. These demands necessitate the extension of earlier results to the spatial model (CR3BP). See Figure 4.
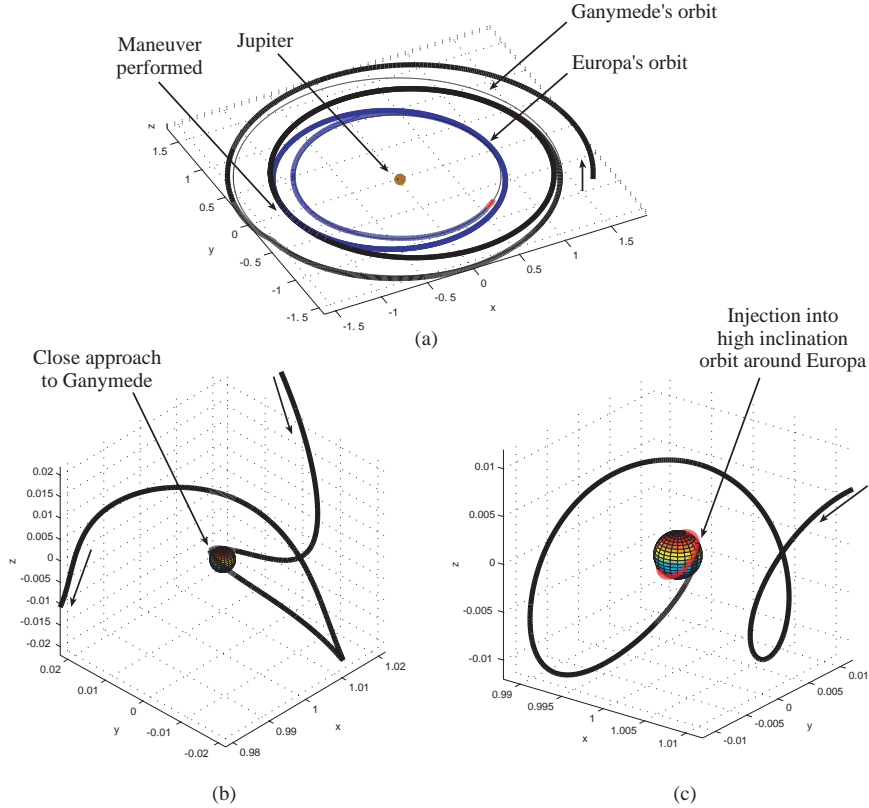

Figure 4:   The three dimensional Petit Grand Tour space mission concept for the Jovian moons. (a) We show a spacecraft trajectory coming into the Jupiter system and transferring from Ganymede to Europa using a single impulsive maneuver, shown in a Jupiter-centered inertial frame. (b) The spacecraft performs one loop around Ganymede, using no propulsion at all, as shown here in the Jupiter-Ganymede rotating frame. (c) The spacecraft arrives in Europa's vicinity at the end of its journey and performs a final propulsion maneuver to get into a high inclination circular orbit around Europa, as shown here in the Jupiter-Europa rotating frame.

In our current work on the spatial three-body problem, we are able to show that the invariant manifold structures of the collinear libration points still act as the separatrices for two types of motion, those inside the invariant manifold "tubes" are transit orbits and those outside the "tubes" are non-transit orbits. We have also designed an algorithm for constructing orbits with any prescribed itinerary and obtained some initial results on the basic itinerary. Furthermore, we have applied the techniques developed in this paper to the construction of a three dimensional Petit Grand Tour of the Jovian moon system. By approximating the dynamics of the Jupiter-Europa-Ganymede-spacecraft 4-body problem as two 3-body subproblems, we seek intersections between the channels of tran-

sit orbits enclosed by the stable and unstable manifold tubes of different moons. In our example, we have designed a low energy transfer trajectory from Ganymede to Europa that ends in a high inclination orbit around Europa.

CIRCULAR RESTRICTED THREE-BODY PROBLEM

The orbital planes of Ganymede and Europa are within $0.3°$ of each other, and their orbital eccentricities are 0.0006 and 0.0101, respectively. Furthermore, since the masses of both moons are small, and they are on rather distant orbits, the coupled spatial CR3BP is an excellent starting model for illuminating the transfer dynamics between these moons. We assume the orbits of Ganymede and Europa are co-planar, but the spacecraft is not restricted to their common orbital plane.

The Spatial Circular Restricted Three Body Problem. We begin by recalling the equations for the circular restricted three-body problem (**CR3BP**). The two main bodies, which we call generically **Jupiter** and the **moon**, have a total mass that is normalized to one. Their masses are denoted by $m_J = 1 - \mu$ and $m_M = \mu$ respectively (see Figure 5(a)). These bodies rotate in the plane counterclockwise about their common center of mass and with the angular velocity normalized to one. The third body, which we call the **spacecraft**, is free to move in the three-dimensional space and its motion is assumed to not affect the primaries. Note that the mass parameters for the Jupiter-Ganymede and Jupiter-Europa systems are $\mu_G = 7.802 \times 10^{-5}$ and $\mu_E = 2.523 \times 10^{-5}$, respectively.

Choose a rotating coordinate system so that the origin is at the center of mass and Jupiter (J) and the moon (M) are fixed on the x-axis at $(-\mu, 0, 0)$ and $(1 - \mu, 0, 0)$ respectively (see Figure 5(a)). Let (x, y, z) be the position of the spacecraft in the rotating frame.

Equations of Motion. There are several ways to derive the equations of motion for this system A efficient technique is to use covariance of the Lagrangian formulation and use the Lagrangian directly in a moving frame.[9] This method gives the equations in Lagrangian form. Then the equations of motion of the spacecraft can be written in second order form as

$$\ddot{x} - 2\dot{y} = \Omega_x, \qquad \ddot{y} + 2\dot{x} = \Omega_y, \qquad \ddot{z} = \Omega_z. \qquad (1)$$

where

$$\Omega(x, y, z) = \frac{x^2 + y^2}{2} + \frac{1 - \mu}{r_1} + \frac{\mu}{r_2} + \frac{\mu(1 - \mu)}{2},$$

where Ω_x, Ω_y, and Ω_z are the partial derivatives of Ω with respect to the variables x, y, and z. Also, $r_1 = \sqrt{(x + \mu)^2 + y^2 + z^2}, r_2 = \sqrt{(x - 1 + \mu)^2 + y^2 + z^2}$. This form of the equations of motion has been studied in detail[10] and are called the equations of the CR3BP.

After applying the Legendre transformation to the Lagrangian formulation, one finds that the Hamiltonian function is given by

$$H = \frac{(p_x + y)^2 + (p_y - x)^2 + p_z^2}{2} - \Omega(x, y, z), \qquad (2)$$

Therefore, Hamilton's equations are given by:

$$\dot{x} = \frac{\partial H}{\partial p_x} = p_x + y, \qquad \dot{p_x} = -\frac{\partial H}{\partial x} = p_y - x + \Omega_x,$$

$$\dot{y} = \frac{\partial H}{\partial p_y} = p_y - x, \qquad \dot{p_y} = -\frac{\partial H}{\partial y} = -p_x - y + \Omega_y,$$

$$\dot{z} = \frac{\partial H}{\partial p_z} = p_z, \qquad \dot{p_z} = -\frac{\partial H}{\partial z} = \Omega_z,$$
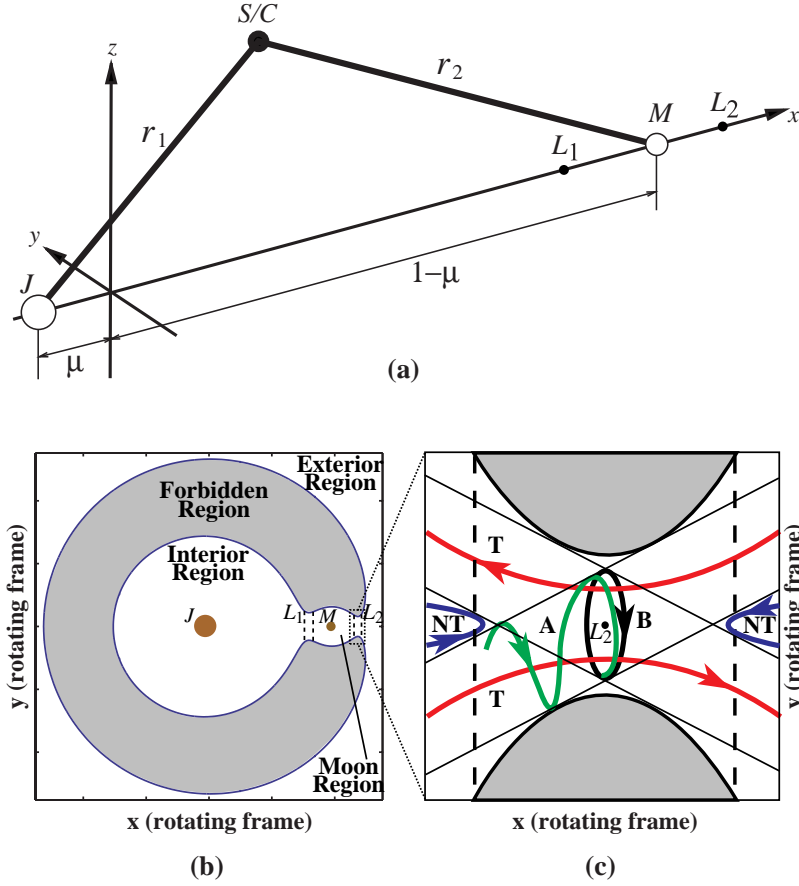
Figure 5: (a) Equilibrium points of the CR3BP as viewed, not in any inertial frame, but in the rotating frame, where Jupiter and a Jovian moon are at fixed positions along the x-axis. (b) Projection of the three-dimensional Hill's region on the (x, y)-plane (schematic, the region in white), which contains a "neck" about L_1 and L_2. (c) The flow in the region near L_2 projected on the (x, y)-plane, showing a bounded orbit around L_2 (labeled B), an asymptotic orbit winding onto the bounded orbit (A), two transit orbits (T) and two non-transit orbits (NT), shown in schematic. A similar figure holds for the region around L_1.

Jacobi Integral. The system (1) have a first integral called the ***Jacobi integral***, which is given by
$$C(x, y, z, \dot{x}, \dot{y}, \dot{z}) = -(\dot{x}^2 + \dot{y}^2 + \dot{z}^2) + 2\Omega(x, y, z) = -2E(x, y, z, \dot{x}, \dot{y}, \dot{z}).$$

We shall use E when we regard the Hamiltonian as a function of the positions and velocities and H when we regard it as a function of the position and mementa.

Equilibrium Points and Hill's Regions. The system (1) has five equilibrium points in the (x, y) plane, 3 collinear ones on the x-axis, called L_1, L_2, L_3 (see Figure 5(a)) and two equilateral points called $L_4 and L_5$. These equilibrium points are critical points of the (effective potential) function Ω. The value of the Jacobi integral at the point L_i will be denoted by C_i.

The level surfaces of the Jacobi constant, which are also ***energy surfaces***, are invariant 5-dimensional manifolds. Let $\mathcal{M}$ be that energy surface, i.e.,

$$\mathcal{M}(\mu, C) = \{(x, y, z, \dot{x}, \dot{y}, \dot{z}) \mid C(x, y, z, \dot{x}, \dot{y}, \dot{z}) = \text{constant}\}$$

6

The projection of this surface onto position space is called a **Hill's region**

$$M(\mu, C) = \{(x, y, z) \mid \Omega(x, y, z) \geq C/2\}.$$

The boundary of $M(\mu, C)$ is the zero velocity curve. The spacecraft can move only within this region. Our main concern here is the behavior of the orbits of equations (1) whose Jacobi constant is just below that of L_2; that is, $C < C_2$. For this case, the three-dimensional Hill's region contains a "neck" about L_1 and L_2, as shown in Figure 5(b). Thus, orbits with a Jacobi constant just below that of L_2 are energetically permitted to make a transit through the two neck regions from the **interior region** (inside the moon's orbit) to the **exterior region** (outside the moon's orbit) passing through the **moon (capture) region**.

INVARIANT MANIFOLD AS SEPARATRIX

Studying the linearization of the dynamics near the equilibria is of course an essential ingredient for understanding the more complete nonlinear dynamics.[4,11,12,13]

Linearization near the Collinear Equilibria. We will denote by $(k, 0, 0, 0, k, 0)$ the coordinates of any of the collinear Lagrange point. To find the linearized equations it, we need the quadratic terms of the Hamiltonian H in equation (2) as expanded about $(k, 0, 0, 0, k, 0)$. After making a coordinate change with $(k, 0, 0, 0, k, 0)$ as the origin, these quadratic terms form the Hamiltonian function for the linearized equations, which we shall call H_l

$$H_l = \frac{1}{2}\{(p_x + y)^2 + (p_y - x)^2 + p_z^2 - ax^2 + by^2 + cz^2\},$$

where, a, b and c are defined by $a = 2\rho + 1$, $b = \rho - 1$, and $c = \rho$ and where

$$\rho = \mu|k - 1 + \mu|^{-3} + (1 - \mu)|k + \mu|^{-3}.$$

A short computation gives the linearized equations in the form

$$\begin{aligned}
\dot{x} &= \frac{\partial H_l}{\partial p_x} = p_x + y, & \dot{p}_x &= -\frac{\partial H_l}{\partial x} = p_y - x + ax, \\
\dot{y} &= \frac{\partial H_l}{\partial p_y} = p_y - x, & \dot{p}_y &= -\frac{\partial H_l}{\partial y} = -p_x - y - by, \\
\dot{z} &= \frac{\partial H_l}{\partial p_z} = p_z, & \dot{p}_z &= -\frac{\partial H_l}{\partial z} = -cz.
\end{aligned}$$

It is straightforward to show that the eigenvalues of this linear system have the form $\pm\lambda$, $\pm i\nu$ and $\pm i\omega$, where λ, ν and ω are positive constants and $\nu \neq \omega$.

To better understand the orbit structure on the phase space, we make a linear change of coordinates with the eigenvectors as the axes of the new system. Using the corresponding new coordinates $q_1, p_1, q_2, p_2, q_3, p_3$, the differential equations assume the simple form

$$\begin{aligned}
\dot{q}_1 &= \lambda q_1, & \dot{p}_1 &= -\lambda p_1, \\
\dot{q}_2 &= \nu p_2, & \dot{p}_2 &= -\nu q_2, \\
\dot{q}_3 &= \omega p_3, & \dot{p}_3 &= -\omega q_3,
\end{aligned} \tag{3}$$

and the Hamiltonian function becomes

$$H_l = \lambda q_1 p_1 + \frac{\nu}{2}(q_2^2 + p_2^2) + \frac{\omega}{2}(q_3^2 + p_3^2). \tag{4}$$

Solutions of the equations (3) can be conveniently written as

$$q_1(t) = q_1^0 e^{\lambda t}, \qquad p_1(t) = p_1^0 e^{-\lambda t},$$
$$q_2(t) + ip_2(t) = (q_2^0 + p_2^0)e^{-i\nu t},$$
$$q_3(t) + ip_2(t) = (q_3^0 + ip_3^0)e^{-i\omega t}, \tag{5}$$

where the constants $q_1^0, p_1^0, q_2^0 + ip_2^0$, and $q_3^0 + ip_3^0$ are the initial conditions. These linearized equations admit integrals in addition to the Hamiltonian function; namely, the functions $q_1 p_1$, $q_2^2 + p_2^2$ and $q_3^2 + p_3^2$ are constant along solutions.

The Linearized Phase Space. For positive h and c, the region $\mathcal{R}$, which is determined by

$$H_l = h, \quad \text{and} \quad |p_1 - q_1| \le c,$$

is homeomorphic to the product of a 4-sphere and an interval I, $S^4 \times I$; namely, for each fixed value of $p_1 - q_1$ between $-c$ and c, we see that the equation $H_l = h$ determines a 4-sphere

$$\frac{\lambda}{4}(q_1 + p_1)^2 + \frac{\nu}{2}(q_2^2 + p_2^2) + \frac{\omega}{2}(q_3^2 + p_3^2) = h + \frac{\lambda}{4}(p_1 - q_1)^2.$$

The bounding 4-sphere of $\mathcal{R}$ for which $p_1 - q_1 = -c$ will be called n_1, and that where $p_1 - q_1 = c$, n_2 (see Figure 6). We shall call the set of points on each bounding 4-sphere where $q_1 + p_1 = 0$ the **equator**, and the sets where $q_1 + p_1 > 0$ or $q_1 + p_1 < 0$ will be called the **north** and **south hemispheres**, respectively.
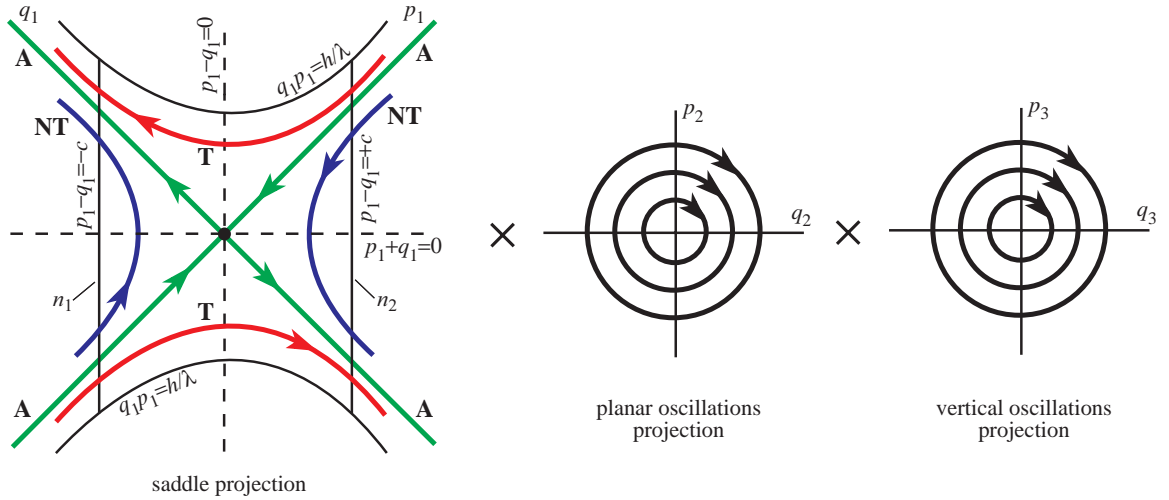

Figure 6: The flow in the equilibrium region has the form saddle × center × center. On the left is shown the projection onto the (p_1, q_1)-plane (note, axes tilted $45°$). Shown are the bounded orbits (black dot at the center), the asymptotic orbits (labeled A), two transit orbits (T) and two non-transit orbits (NT).

The Linear Flow in $\mathcal{R}$. To analyze the flow in $\mathcal{R}$, one considers the projections on the (q_1, p_1)-plane and $(q_2, p_2) \times (q_3, p_3)$-space, respectively. In the first case we see the standard picture of an unstable critical point, and in the second, of a center consisting of two uncoupled harmonic oscillators. Figure 6 schematically illustrates the flow. The coordinate axes of the (q_1, p_1)-plane have been tilted by $45°$ and labeled (p_1, q_1) instead in order to correspond to the direction of the

8

flow in later figures which adopt the NASA convention that the larger primary is to the left of the small primary. With regard to the first projection we see that $\mathcal{R}$ itself projects to a set bounded on two sides by the hyperbola $q_1 p_1 = h/\lambda$ (corresponding to $q_2^2 + p_2^2 = q_3^2 + p_3^2 = 0$, see (4)) and on two other sides by the line segments $p_1 - q_1 = \pm c$, which correspond to the bounding 4-spheres.

Since $q_1 p_1$ is an integral of the equations in $\mathcal{R}$, the projections of orbits in the (q_1, p_1)-plane move on the branches of the corresponding hyperbolas $q_1 p_1 = $ constant, except in the case $q_1 p_1 = 0$, where $q_1 = 0$ or $p_1 = 0$. If $q_1 p_1 > 0$, the branches connect the bounding line segments $p_1 - q_1 = \pm c$ and if $q_1 p_1 < 0$, they have both end points on the same segment. A check of equation (5) shows that the orbits move as indicated by the arrows in Figure 6.

To interpret Figure 6 as a flow in $\mathcal{R}$, notice that each point in the (q_1, p_1)-plane projection corresponds to a 3-sphere S^3 in $\mathcal{R}$ given by

$$\frac{\nu}{2}(q_2^2 + p_2^2) + \frac{\omega}{2}(q_3^2 + p_3^2) = h - \lambda q_1 p_1.$$

Of course, for points on the bounding hyperbolic segments $(q_1 p_1 = h/\lambda)$, the 3-sphere collapses to a point. Thus, the segments of the lines $p_1 - q_1 = \pm c$ in the projection correspond to the 4-spheres bounding $\mathcal{R}$. This is because each corresponds to a 3-sphere crossed with an interval where the two end 3-spheres are pinched to a point.

We distinguish nine classes of orbits grouped into the following four categories:

1. The point $q_1 = p_1 = 0$ corresponds to an invariant 3-sphere S_h^3 of **bounded orbits** (periodic and quasi-periodic) in $\mathcal{R}$. This 3-sphere is given by

   $$\frac{\nu}{2}(q_2^2 + p_2^2) + \frac{\omega}{2}(q_3^2 + p_3^2) = h, \qquad q_1 = p_1 = 0.$$

   It is an example of a ***normally hyperbolic invariant manifold*** (NHIM).[14] Roughly, this means that the stretching and contraction rates under the linearized dynamics transverse to the 3-sphere dominate those tangent to the 3-sphere. This is clear for this example since the dynamics normal to the 3-sphere are described by the exponential contraction and expansion of the saddle point dynamics. Here the 3-sphere acts as a "big saddle point". See the black dot at center the (q_1, p_1)-plane on the left side of Figure 6.

2. The four half open segments on the axes, $q_1 p_1 = 0$, correspond to four cylinders of orbits asymptotic to this invariant 3-sphere S_h^3 either as time increases ($p_1 = 0$) or as time decreases ($q_1 = 0$). These are called ***asymptotic*** orbits and they form the stable and the unstable manifolds of S_h^3. The ***stable manifolds***, $W^s(S_h^3)$, are given by

   $$\frac{\nu}{2}(q_2^2 + p_2^2) + \frac{\omega}{2}(q_3^2 + p_3^2) = h, \qquad q_1 = 0.$$

   The unstable manifolds, $W^s(S_h^3)$, are given by

   $$\frac{\nu}{2}(q_2^2 + p_2^2) + \frac{\omega}{2}(q_3^2 + p_3^2) = h, \qquad p_1 = 0.$$

   Topologically, both invariant manifolds look like 4-dimensional "tubes" $(S^3 \times \mathbb{R})$. See the four orbits labeled A of Figure 6.

3. The hyperbolic segments determined by $q_1 p_1 = $ constant > 0 correspond to two cylinders of orbits which cross $\mathcal{R}$ from one bounding 4-sphere to the other, meeting both in the same hemisphere; the northern hemisphere if they go from $p_1 - q_1 = +c$ to $p_1 - q_1 = -c$, and the southern hemisphere in the other case. Since these orbits transit from one region to another, we call them ***transit*** orbits. See the two orbits labeled T of Figure 6.

4. Finally the hyperbolic segments determined by $q_1 p_1 = \text{constant} < 0$ correspond to two cylinders of orbits in $\mathcal{R}$ each of which runs from one hemisphere to the other hemisphere on the same bounding 4-sphere. Thus if $q_1 > 0$, the 4-sphere is n_1 ($p_1 - q_1 = -c$) and orbits run from the southern hemisphere ($q_1 + p_1 < 0$) to the northern hemisphere ($q_1 + p_1 > 0$) while the converse holds if $q_1 < 0$, where the 4-sphere is n_2. Since these orbits return to the same region, we call them ***non-transit*** orbits. See the two orbits labeled NT of Figure 6.

McGehee Representation. As noted above, $\mathcal{R}$ is a 5-dimensional manifold that is homeomorphic to $S^4 \times I$. It can be represented by a spherical annulus bounded by two 4-spheres n_1, n_2, as shown in Figure 7(b). Figure 7(a) is a cross-section of $\mathcal{R}$. Notice that this cross-section is qualitatively
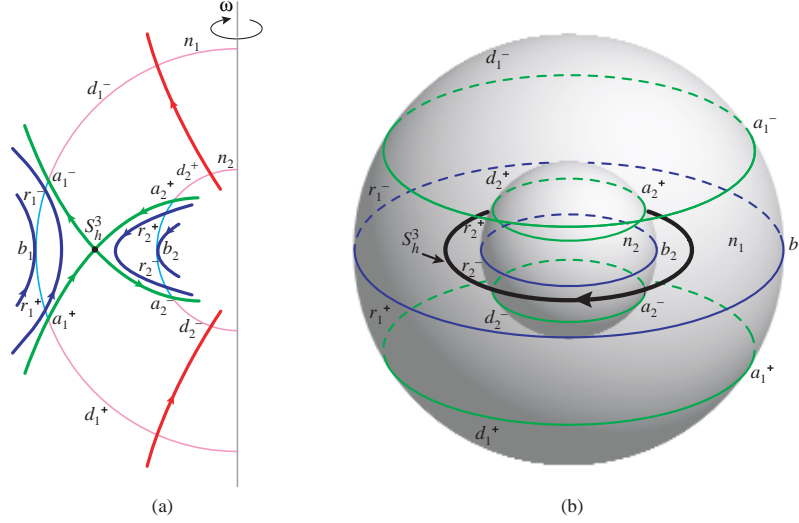

(a)   (b)

Figure 7: (a) The cross-section of the flow in the $\mathcal{R}$ region of the energy surface. (b) The McGehee representation of the flow in the region $\mathcal{R}$.

the same as the illustration in Figure 6. The following classifications of orbits correspond to the previous four categories:

1. There is an invariant 3-sphere S_h^3 of bounded orbits in the region $\mathcal{R}$ corresponding to the point l. Notice that this 3-sphere is the equator of the central 4-sphere given by $p_1 - q_1 = 0$.

2. Again let n_1, n_2 be the bounding 4-spheres of region $\mathcal{R}$, and let n denote either n_1 or n_2. We can divide n into two hemispheres: n^+, where the flow enters $\mathcal{R}$, and n^-, where the flow leaves $\mathcal{R}$. There are four cylinders of orbits *asymptotic* to the invariant 3-sphere S_h^3. They form the stable and unstable manifolds to the invariant 3-sphere S_h^3. Let a^+ and a^- (where $q_1 = 0$ and $p_1 = 0$ respectively) be the intersections with n of the stable and unstable manifolds. Then a^+ appears as a 3-sphere in n^+, and a^- appears as a 3-sphere in n^-.

3. Consider the two spherical caps on each bounding 4-sphere given by

$$d_1^+ = \{(q_1, p_1, q_2, p_2, q_3, p_3) \mid \ p_1 - q_1 = -c, \ q_1 < 0\},$$
$$d_1^- = \{(q_1, p_1, q_2, p_2, q_3, p_3) \mid \ p_1 - q_1 = -c, \ p_1 > 0\},$$
$$d_2^+ = \{(q_1, p_1, q_2, p_2, q_3, p_3) \mid \ p_1 - q_1 = +c, \ q_1 > 0\},$$
$$d_1^- = \{(q_1, p_1, q_2, p_2, q_3, p_3) \mid \ p_1 - q_1 = +c, \ p_1 < 0\}.$$

If we let d_1^+ be the spherical cap in n_1^+ bounded by a_1^+, then the *transit* orbits entering $\mathcal{R}$ on d_1^+ exit on d_2^- of the other bounding sphere. Similarly, letting d_1^- be the spherical cap in n_1^- bounded by a_1^-, the transit orbits leaving on d_1^- have come from d_2^+ on the other bounding sphere.

4. Note that the intersection b (where $q_1 + p_1 = 0$) of n^+ and n^- is a 3-sphere of tangency points. Orbits tangent at this 3-sphere "bounce off," i.e., do not enter $\mathcal{R}$ locally. Moreover, if we let r^+ be a spherical zone which is bounded by a^+ and b, then *non-transit* orbits entering $\mathcal{R}$ on r^+ exit on the same bounding 4-sphere through r^- which is bounded by a^- and b.

Invariant Manifolds as Separatrices. The key observation here is that the asymptotic orbits form 4-dimensional stable and unstable manifold "tubes" ($S^3 \times \mathbb{R}$) to the invariant 3-sphere S_h^3 in a 5-dimensional energy surface and they separate two distinct types of motion: transit orbits and non-transit orbits. The transit orbits, passing from one region to another, are those inside the 4-dimensional manifold tube. The non-transit orbits, which bounce back to their region of origin, are those outside the tube.

In fact, it can be shown that for a value of Jacobi constant just below that of L_1 (L_2), the nonlinear dynamics in the equilibrium region $\mathcal{R}_1$ ($\mathcal{R}_2$) is qualitatively the same as the linearized picture that we have shown above.[15,16,17] This geometric insight will be used below to guide our numerical explorations in constructing orbits with prescribed itineraries.

Construction of Orbits with Prescribed Itineraries in the Planar Case

In previous work on the planar case,[4] a numerical demonstration is given of a **heteroclinic connection** between pairs of equal Jacobi constant Lyapunov orbits, one around L_1, the other around L_2. This heteroclinic connection augments the homoclinic orbits associated with the L_1 and L_2 Lyapunov orbits, which were previously known.[12] Linking these heteroclinic connections and homoclinic orbits leads to **dynamical chains**.
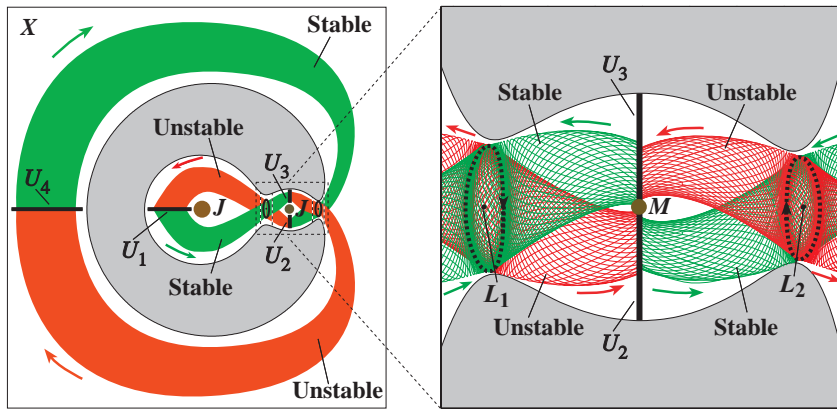

Figure 8: Location of Lagrange point orbit invariant manifold tubes in position space. Stable manifolds are lightly shaded, unstable manifolds are darkly. The location of the Poincaré sections (U_1, U_2, U_3, and U_4) are also shown.

We proved the existence of a large class of interesting orbits near a chain which a spacecraft can follow in its rapid transition between the inside and outside of a Jovian moon's orbit via a moon encounter. The global collection of these orbits is called a **dynamical channel**. We proved a theorem which gives the global orbit structure in the neighborhood of a chain. In simplified form, the theorem essentially says:

11

For any admissible bi-infinite sequence $(\ldots, u_{-1}; u_0, u_1, u_2, \ldots)$ of symbols $\{I, M, X\}$ where I, M, and X stand for the interior, moon, and exterior regions respectively, there corresponds an orbit near the chain whose past and future whereabouts with respect to these three regions match those of the given sequence.

For example, consider the Jupiter-Ganymede-spacecraft 3-body system. Given the bi-infinite sequence $(\ldots, I; M, X, M, \ldots)$, there exists an orbit starting in the Ganymede region which came from the interior region and is going to the exterior region and returning to the Ganymede region.

Moreover, we not only proved the existence of orbits with prescribed itineraries, but develop a systematic procedure for their numerical construction. We will illustrate below the numerical construction of orbits with prescribed finite (but arbitrarily large) itineraries in the three-body planet-moon-spacecraft problem. As our example, chosen for simplicity of exposition, we construct a spacecraft orbit with the central block $(M, X; M, I, M)$. See Figures 9(a) and 9(b).
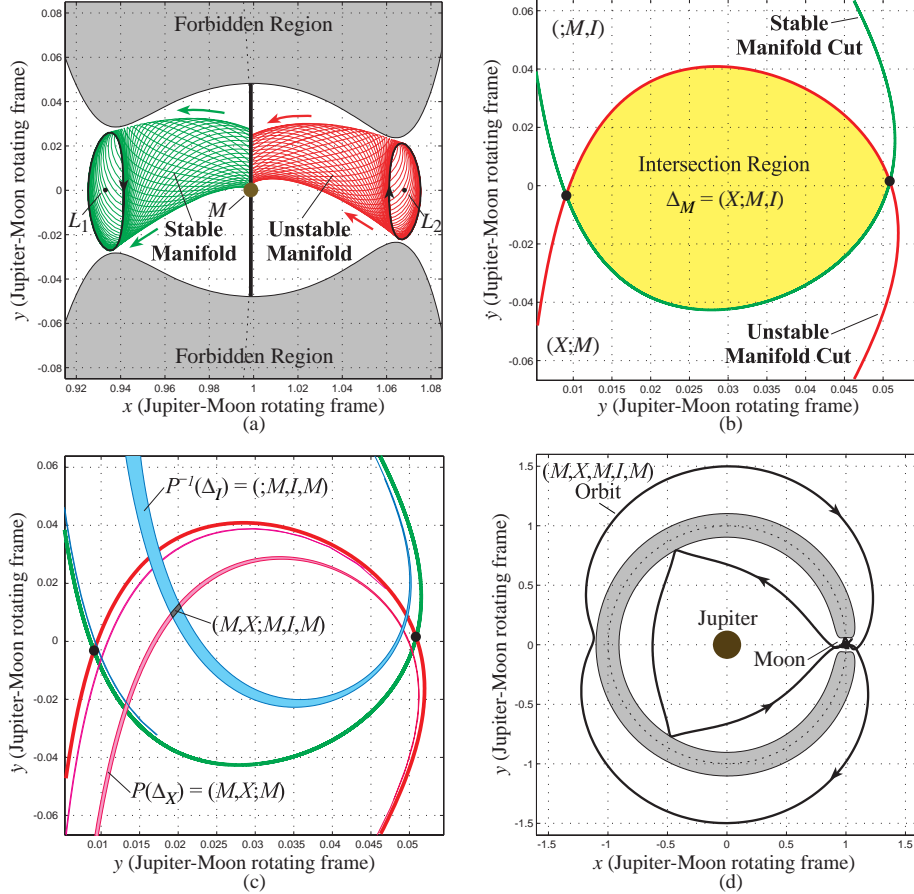

Figure 9: (a) The projection of invariant manifolds $W^{s, \mathcal{M}}_{L_1, \text{p.o.}}$ and $W^{u, \mathcal{M}}_{L_2, \text{p.o.}}$ in the region M of the position space. (b) A close-up of the intersection region between the Poincaré cuts of the invariant manifolds on the U_3 section ($x = 1 - \mu, y > 0$). (c) Intersection between image of Δ_X and pre-image of Δ_I labeled $(M, X; M, I, M)$. (d) Example orbit passing through $(M, X; M, I, M)$ region of (c).

Example Itinerary: $(M, X; M, I, M)$. For the present numerical construction, we adopt the following convention. The U_1 and U_4 Poincaré sections will be $(y = 0, x < 0, \dot{y} < 0)$ in the interior

region, and $(y = 0, x < -1, \dot{y} > 0)$ in the exterior region, respectively. The U_2 and U_3 sections will be $(x = 1 - \mu, y < 0, \dot{x} > 0)$ and $(x = 1 - \mu, y > 0, \dot{x} < 0)$ in the moon region, respectively. See Figure 8 for the location of the Poincaré sections relative to the tubes.

A key observation for the planar case is a result which has shown that the invariant manifold tubes separate two types of motion. The orbits inside the tube transit from one region to another; those outside the tubes bounce back to their original region.

Since the upper curve in Figure 9(b) is the Poincaré cut of the stable manifold of the periodic orbit around L_1 in the U_3 plane, a point inside that curve is an orbit that goes from the moon region to the interior region, so this region can be described by the label $(; M, I)$. Similarly, a point inside the lower curve of Figure 9(b) came from the exterior region into the moon region, and so has the label $(X; M)$. A point inside the intersection $\Delta_{\mathcal{M}}$ of *both* curves is an $(X; M, I)$ orbit, so it makes a transition from the exterior region to the interior region, passing through the moon region. Similarly, by choosing Poincaré sections in the interior and the exterior region, i.e., in the U_1 and U_4 plane, we find the intersection region $\Delta_{\mathcal{I}}$ consisting of $(M; I, M)$ orbits, and $\Delta_{\mathcal{X}}$, which consists of $(M; X, M)$ orbits.

Flowing the intersection $\Delta_{\mathcal{X}}$ forward to the moon region, it stretches into the strips in Figure 9(c). These strips are the image of $\Delta_{\mathcal{X}}$ (i.e., $P(\Delta_{\mathcal{X}})$) under the Poincaré map P, and thus get the label $(M, X; M)$. Similarly, flowing the intersection Δ_I backward to the moon region, it stretches into the strips $P^{-1}(\Delta_{\mathcal{I}})$ in Figure 9(c), and thus have the label $(; M, I, M)$. The intersection of these two types of strips (i.e., $\Delta_{\mathcal{M}} \cap P(\Delta_{\mathcal{X}}) \cap P^{-1}(\Delta_{\mathcal{I}})$) consist of the desired $(M, X; M, I, M)$ orbits. If we take any point inside these intersections and integrate it forward and backward, we find the desired orbits. See Figure 9(d).

Extension of Results in Planar Model to Spatial Model

Since the key step in the planar case is to find the intersection region inside the two Poincaré cuts, a key difficulty is to determine how to extend this technique to the spatial case. Take as an example the construction of a transit orbit with the itinerary $(X; M, I)$ that goes from the exterior region to the interior region of the Jupiter-moon system. Recall that in the spatial case, the unstable manifold "tube" of the NHIM around L_2 which separates the transit and non-transit orbits is topologically $S^3 \times \mathbb{R}$. For a transversal cut at $x = 1 - \mu$ (a hyperplane through the moon), the Poincaré cut is a topological 3-sphere S^3 (in $\mathbb{R}^4$). It is not obvious how to find the intersection region inside these two Poincaré cuts (S^3) since both its projections on the $(y, \dot{y})$-plane and the $(z, \dot{z})$-plane are (2-dimensional) disks D^2. (One easy way to visualize this is to look at the equation: $\xi^2 + \dot{\xi}^2 + \eta^2 + \dot{\eta}^2 = r^2 = r_\xi^2 + r_\eta^2$. that describes a 3-sphere in $\mathbb{R}^4$. Clearly, its projections on the $(\xi, \dot{\xi})$-plane and the $(\eta, \dot{\eta})$-plane are 2-disks as r_ξ and r_η vary from 0 to r and from r to 0 respectively.)

However, in constructing an orbit which transitions from the outside to the inside of a moon's orbit, suppose that we might also want it to have other characteristics above and beyond this gross behavior. We may want to have an orbit which has a particular z-amplitude when it is near the moon. If we set $z = c, \dot{z} = 0$ where c is the desired z-amplitude, the problem of finding the intersection region inside two Poincaré cuts suddenly becomes tractable. Now, the projection of the Poincaré cut of the above unstable manifold tube on the $(y, \dot{y})$-plane will be a closed curve and any point inside this curve is a $(X; M)$ orbit which has transited from the exterior region to the moon region passing through the L_2 equilibrium region. See Figure 10.

Similarly, we can apply the same techniques to the Poincaré cut of the stable manifold tube to the NHIM around L_1 and find all (M, I) orbits inside a closed curve in the $(y, \dot{y})$-plane. Hence, by using z and $\dot{z}$ as the additional parameters, we can apply the similar techniques that we have developed for the planar case in constructing spatial trajectories with desired itineraries. See Figures 11, 12 and 13. What follows is a more detailed description.
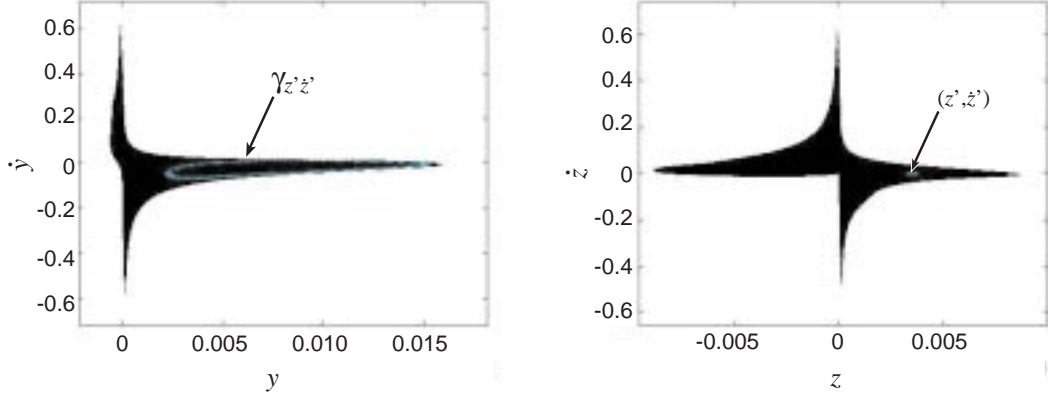
Figure 10: Shown in black are the $y\dot{y}$ (left) and $z\dot{z}$ (right) projections of the 3-dimensional object $\mathcal{C}_1^{+u2}$, the intersection of $W_+^u(\mathcal{M}_h^2)$ with the Poincaré section $x = 1-\mu$. The set of points in the $y\dot{y}$ projection which approximate a curve, $\gamma_{z'\dot{z}'}$, all have $(z, \dot{z})$ values within the small box shown in the $z\dot{z}$ projection (which appears as a thin strip), centered on $(z', \dot{z}')$. This example is computed in the Jupiter-Europa system for $C = 3.0028$.
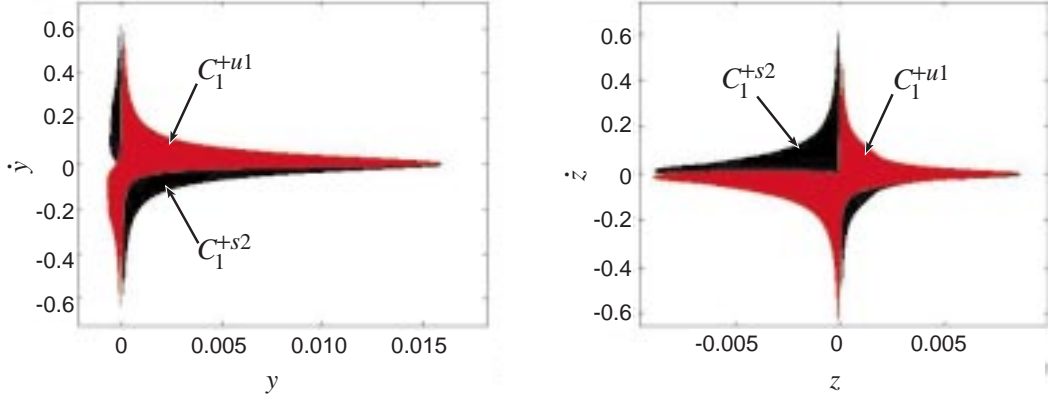

Figure 11: The $y\dot{y}$ (left) and $z\dot{z}$ (right) projections of the 3-dimensional objects $\mathcal{C}_1^{+u2}$ and $\mathcal{C}_1^{+s1}$. This example is computed in the Jupiter-Europa system for $C = 3.0028$.

Finding the Poincaré Cuts. We begin with the 15th order normal form expansion near L_1 and L_2.[18,19,20] The behavior of orbits in the coordinate system of that normal form, $(q_1, p_1, q_2, p_2, q_3, p_3)$, are qualitatively similar to the behavior of orbits in the linear approximation. This makes the procedure for choosing initial conditions in the L_1 and L_2 equilibrium regions rather simple. In particular, based on our knowledge of the structure for the linear system, we can pick initial conditions which produce a close "shadow" of the stable and unstable manifold "tubes" ($S^3 \times \mathbb{R}$) associated to the normally hyperbolic invariant manifold (NHIM), also called central or neutrally stable manifold, in both the L_1 and L_2 equilibrium regions. As we restrict to an energy surface with energy h, there is only one NHIM per energy surface, denoted $\mathcal{M}_h(\simeq S^3)$.

The initial conditions in $(q_1, p_1, q_2, p_2, q_3, p_3)$ are picked with the qualitative picture of the linear system in mind. The coordinates (q_1, p_1) correspond to the saddle projection, (q_2, p_2) correspond to oscillations within the (x, y) plane, and (q_3, p_3) correspond to oscillations within the z direction. Also note that $q_3 = p_3 = 0$ ($z = \dot{z} = 0$) corresponds to an invariant manifold of the system, i.e., the planar system is an invariant manifold of the three degree of freedom system.
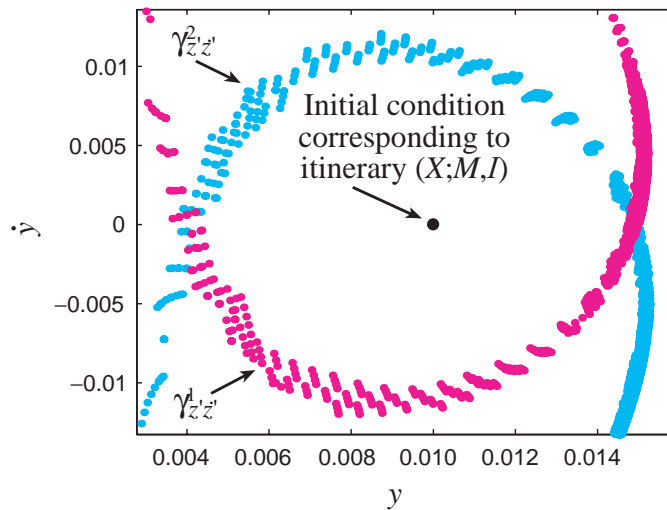
Figure 12: On the $(y, \dot{y})$-plane are shown the points that approximate $\gamma^2_{z'\dot{z}'}$ and $\gamma^1_{z'\dot{z}'}$, the boundaries of int$(\gamma^2_{z'\dot{z}'})$ and int$(\gamma^1_{z'\dot{z}'})$, respectively, where $(z', \dot{z}') = (0.0035, 0)$. Note the lemon shaped region of intersection, int$(\gamma^1_{z'\dot{z}'}) \cap$ int$(\gamma^2_{z'\dot{z}'})$, in which all orbits have the itinerary $(X; M, I)$. The appearance is similar to Figure 9(b). The point shown within int$(\gamma^1_{z'\dot{z}'}) \cap$ int$(\gamma^2_{z'\dot{z}'})$ is the initial condition for the orbit shown in Figure 13.

The initial conditions to approximate the stable and unstable manifolds $(W^s_\pm(\mathcal{M}_h), W^u_\pm(\mathcal{M}_h))$ are picked via the following procedure. Note that we can be assured that we are obtaining a roughly complete approximation of points along a slice of $W^s_\pm(\mathcal{M}_h)$ and $W^u_\pm(\mathcal{M}_h)$ since such a slice is compact, having the structure S^3. Also, we know roughly the picture from the linear case.

1. We fix $q_1 = p_1 = \pm\epsilon$, where ϵ is small. This ensures that almost all of the initial conditions will be for orbits which are transit orbits from one side of the equilibrium region to the other. Specifically $+$ corresponds to right-to-left transit orbits and $-$ corresponds to left-to-right transit orbits. We choose ϵ small so that the initial conditions are near the NHIM $\mathcal{M}_h$ (at $q_1 = p_1 = 0$) and will therefore integrate forward and backward to be near the unstable and stable manifold of $\mathcal{M}_h$, respectively. We choose ϵ to not be too small, or the integrated orbits will take too long to leave the vicinity of $\mathcal{M}_h$.

2. Beginning with $r_v = 0$, and increasing incrementally to some maximum $r_v = r_v^{\max}$, we look for initial conditions with $q_3^2 + p_3^2 = r_v^2$, i.e. along circles in the z oscillation canonical plane. It is reasonable to look along circles centered on the origin $(q_3, p_3) = (0, 0)$ on this canonical plane since the motion is simple harmonic in the linear case and the origin corresponds to an invariant manifold.

3. For each point along the circle, we look for the point on the energy surface in the (q_2, p_2) plane, i.e., the (x, y) oscillation canonical plane. Note, our procedure can tell us if such a point exists and clearly if no point exists, it will not used as an initial condition.

After picking the initial conditions in $(q_1, p_1, q_2, p_2, q_3, p_3)$ coordinates, we transform to the conventional CR3BP coordinates $(x, y, z, \dot{x}, \dot{y}, \dot{z})$ and integrate under the full equations of motion. The integration proceeds until some Poincaré section stopping condition is reached, for example $x = 1 - \mu$. We can then use further analyses on the Poincaré section, described below.

Example Itinerary: $(X; M, I)$. As an example, suppose we want a transition orbit going from outside to inside the moon's orbit in the Jupiter-moon system. We therefore want right-to-left
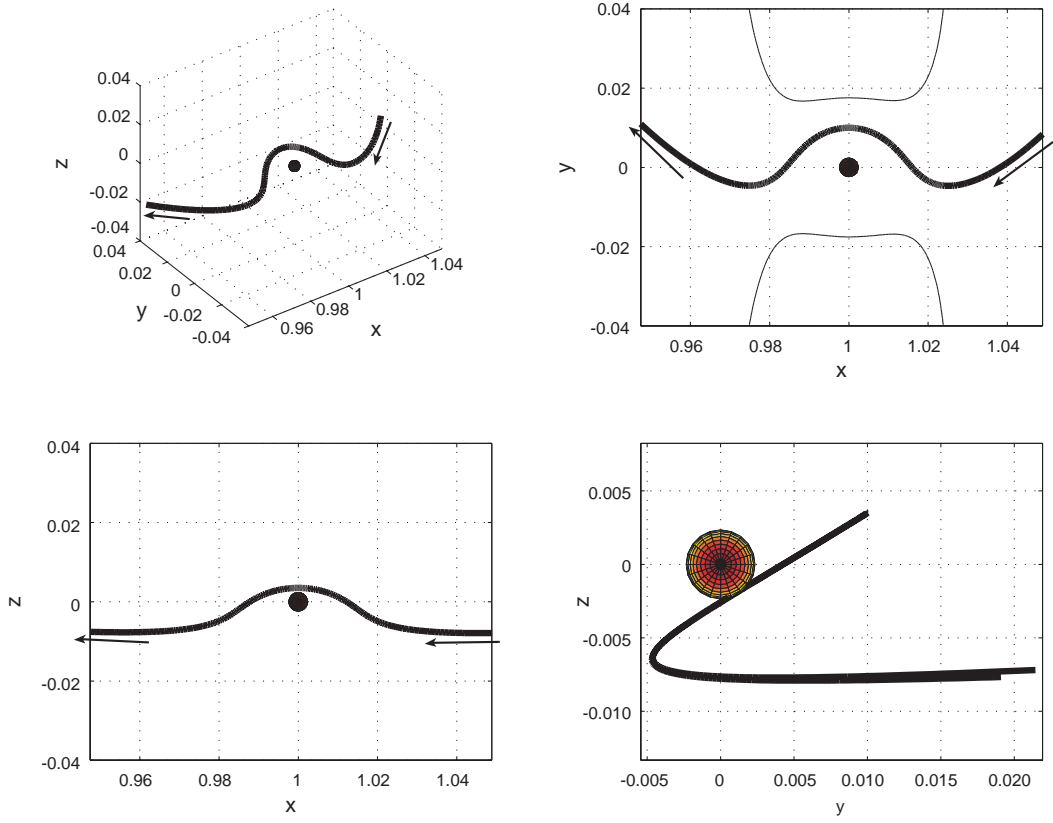
15

Figure 13: The (X, M, I) transit orbit corresponding to the initial condition in Figure 12. The orbit is shown in a 3D view and in the three orthographic projections. Europa is shown to scale. The upper right plot includes the $z = 0$ section of the zero velocity surface (compare with Figure 5(b)).

transit orbits in both the L_1 and L_2 equilibrium regions. Consider the L_2 side. The set of right-to-left transit orbits has the structure $D^4 \times \mathbb{R}$ (where D^4 is a 4-dimensional disk), with boundary $S^3 \times \mathbb{R}$. The boundary is made up of $W^s_+(\mathcal{M}^2_h)$ and $W^u_+(\mathcal{M}^2_h)$, where the $+$ means right-to-left, $\mathcal{M}^2_h$ is the NHIM around L_2 with energy h, and 2 denotes L_2. We pick the initial conditions to approximate $W^s_+(\mathcal{M}^2_h)$ and $W^u_+(\mathcal{M}^2_h)$ as outlined above and then integrate those initial conditions forward in time until they intersect the Poincaré section at $x = 1 - \mu$, a hyperplane passing through the center of the moon.

Since the Hamiltonian energy h (Jacobi constant) is fixed, the set of all values $\mathcal{C} = \{(y, \dot{y}, z, \dot{z})\}$ obtained at the Poincaré section, characterize the branch of the manifold of all Lagrange point orbits around the selected equilibrium point for the particular section. Let us denote the set as $\mathcal{C}^{+uj}_i$, where $+$ denotes the right-to-left branch of the s (stable) or u (unstable) manifold of the L_j, $j = 1, 2$ Lagrange point orbits at the i-th intersection with $x = 1 - \mu$. We will look at the first intersection, so we have $\mathcal{C}^{+u2}_1$.

The object $\mathcal{C}^{+u2}_1$ is 3-dimensional ($\simeq S^3$) in the 4-dimensional $(y, \dot{y}, z, \dot{z})$ space. For the Jupiter-Europa system, we show $\mathcal{C}^{+u2}_1$ for Jacobi constant $C = 3.0028$ in Figure 10.

Thus, we suspect that if we pick almost any point $(z', \dot{z}')$ in the $z\dot{z}$ projection, it corresponds to a closed loop $\gamma_{z'\dot{z}'}$ ($\simeq S^1$) in the $y\dot{y}$ projection (see Figure 10). Any initial condition $(y', \dot{y}', z', \dot{z}')$, where $(y', \dot{y}') \in \gamma_{z'\dot{z}'}$ will be on $W^u_+(\mathcal{M}^2_h)$, and will wind onto a Lagrange point orbit when integrated backwards in time. Thus, $\gamma_{z'\dot{z}'}$ defines the boundary of right-to-left transit orbits with $(z, \dot{z}) = (z', \dot{z}')$. If we choose $(y', \dot{y}') \in \text{int}(\gamma_{z'\dot{z}'})$ where $\text{int}(\gamma_{z'\dot{z}'})$ is the region in the $y\dot{y}$ projection enclosed

by $\gamma_{z'\dot{z}'}$, then the initial condition $(y', \dot{y}', z', \dot{z}')$ will correspond to a right-to-left transit orbit, which will pass through the L_2 equilibrium region, from the moon region to outside the moon's orbit, when integrated backward in time.

Similarly, on the L_1 side, we pick the initial conditions to approximate $W_+^s(\mathcal{M}_h^1)$ and $W_+^u(\mathcal{M}_h^1)$ as outlined above and then integrate those initial conditions backward in time until they intersect the Poincaré section at $x = 1 - \mu$, obtaining $\mathcal{C}_1^{+s1}$. We can do a similar construction regarding transit orbits, etc. To distinguish closed loops $\gamma_{z'\dot{z}'}$ from L_1 or L_2, let us call a loop $\gamma_{z'\dot{z}'}^j$ if it is from $L_j, j = 1, 2$.

To find initial conditions for transition orbits which go from outside the moon's orbit to inside the moon's orbit with respect to Jupiter, i.e. orbits which are right-to-left transit orbits in both the L_1 and L_2 equilibrium regions, we need to look at the intersections of the interiors of $\mathcal{C}_1^{+u2}$ and $\mathcal{C}_1^{+s1}$. See Figure 11.

To find such initial conditions we first look for intersections in the $z\dot{z}$ projection. Consider the projection $\pi_{z\dot{z}} : \mathbb{R}^4 \to \mathbb{R}^2$ given by $(y, \dot{y}, z, \dot{z}) \mapsto (z, \dot{z})$. Consider a point $(y', \dot{y}', z', \dot{z}') \in \pi_{z\dot{z}}(\mathcal{C}_1^{+u2}) \cap \pi_{z\dot{z}}(\mathcal{C}_1^{+s1}) \neq \varnothing$, i.e. a point $(y', \dot{y}', z', \dot{z}')$ where $(z', \dot{z}')$ is in the intersection of the $z\dot{z}$ projections of $\mathcal{C}_1^{+u2}$ and $\mathcal{C}_1^{+s1}$. Transit orbits from outside to inside the moon's orbit are such that $(y', \dot{y}', z', \dot{z}') \in$ int$(\gamma_{z'\dot{z}'}^1) \cap$ int$(\gamma_{z'\dot{z}'}^2)$. If int$(\gamma_{z'\dot{z}'}^1) \cap$ int$(\gamma_{z'\dot{z}'}^2) = \varnothing$, then no transition exists for that value of $(z', \dot{z}')$. But numerically we find that there are values of $(z', \dot{z}')$ such that int$(\gamma_{z'\dot{z}'}^1) \cap$ int$(\gamma_{z'\dot{z}'}^2) \neq \varnothing$. See Figures 11 and 12.

In essence we are doing a search for transit orbits by looking at a two parameter set of intersections of the interiors of closed curves, $\gamma_{z\dot{z}}^1$ and $\gamma_{z\dot{z}}^2$ in the $y\dot{y}$ projection, where our two parameters are given by $(z, \dot{z})$. Furthermore, we can reduce this to a one parameter family of intersections by restricting to $\dot{z} = 0$. This is a convenient choice since it implies that the orbit is at a critical point (often a maximum or minimum in z when it reaches the surface $x = 1 - \mu$.)

Technically, we are not able to look at curves $\gamma_{z\dot{z}}^j$ belonging to points $(z, \dot{z})$ in the $z\dot{z}$ projection. Since we are approximating the 3-dimensional surface $\mathcal{C}$ by a scattering of points (about a million for the computations in this paper), we must look not at points $(z, \dot{z})$, but at small boxes $(z \pm \delta z, \dot{z} \pm \delta \dot{z})$ where δz and $\delta \dot{z}$ are small. Since our box in the $z\dot{z}$ projection has a finite size, the points in the $y\dot{y}$ projection corresponding to the points in the box will not all fall on a close curve, but along a slightly broadened curve, a strip, as seen in Figure 12. For our purposes, we will still refer to the collection of such points as $\gamma_{z\dot{z}}^j$.

Transfer from Ganymede to High Inclination Europa Orbit.

Petit Grand Tour. We now apply the techniques we have developed to the construction of a fully three dimensional Petit Grand Tour of the Jovian moons, extending an earlier planar result.[7] We here outline how one systematically constructs a spacecraft tour which begins beyond Ganymede in orbit around Jupiter, makes a close flyby of Ganymede, and finally reaches a high inclination orbit around Europa, consuming less fuel than is possible from standard two-body methods.

Our approach involves the following three key ideas:

1. treat the Jupiter-Ganymede-Europa-spacecraft 4-body problem as two coupled circular restricted 3-body problems, the Jupiter-Ganymede-spacecraft and Jupiter-Europa-spacecraft systems;

2. use the stable and unstable manifolds of the NHIMs about the Jupiter-Ganymede L_1 and L_2 to find an uncontrolled trajectory from a jovicentric orbit beyond Ganymede to a temporary capture around Ganymede, which subsequently leaves Ganymede's vicinity onto a jovicentric orbit interior to Ganymede's orbit;

3. use the stable manifold of the NHIM around the Jupiter-Europa L_2 to find an uncontrolled trajectory from a jovicentric orbit between Ganymede and Europa to a temporary capture

around Europa. Once the spacecraft is temporarily captured around Europa, a propulsion maneuver can be performed when its trajectory is close to Europa (100 km altitude), taking it into a high inclination orbit about the moon. Furthermore, a propulsion maneuver will be needed when transferring from the Jupiter-Ganymede portion of the trajectory to the Jupiter-Europa portion, since the respective transport tubes exist at different energies.

Ganymede to Europa Transfer Mechanism. The construction begins with the patch point, where we connect the Jupiter-Ganymede and Jupiter-Europa portions, and works forward and backward in time toward each moon's vicinity. The construction is done mainly in the Jupiter-Europa rotating frame using a Poincaré section. After selecting appropriate energies in each 3-body system, respectively, the stable and unstable manifolds of each system's NHIMs are computed. Let $^{\mathrm{Gan}}W^u_+(\mathcal{M}^1)$ denote the unstable manifold of Ganymede's L_1 NHIM and $^{\mathrm{Eur}}W^s_+(\mathcal{M}^2)$ denote the stable manifold for Europa's. L_2 NHIM. We look at the intersection of $^{\mathrm{Gan}}W^u_+(\mathcal{M}^1)$ and $^{\mathrm{Eur}}W^s_+(\mathcal{M}^2)$ with a common Poincaré section, the surface U_1 in the Jupiter-Europa rotating frame, defined earlier. See Figure 14.
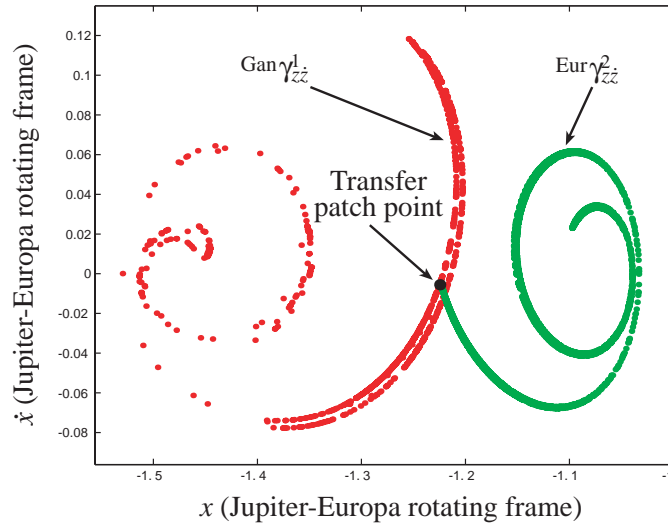

Figure 14: The curves $^{\mathrm{Gan}}\gamma^1_{z\dot{z}}$ and $^{\mathrm{Eur}}\gamma^2_{z\dot{z}}$ are shown, the intersections of $^{\mathrm{Gan}}W^u_+(\mathcal{M}^1)$ and $^{\mathrm{Eur}}W^s_+(\mathcal{M}^2)$ with the Poincaré section U_1 in the Jupiter-Europa rotating frame, respectively. Note the small region of intersection, $\mathrm{int}(\mathrm{Gan}\gamma^1_{z\dot{z}}) \cap \mathrm{int}(^{\mathrm{Eur}}\gamma^2_{z\dot{z}})$, where the patch point is labeled.

Note that we have the freedom to choose where the Poincaré section is with respect to Ganymede, which determines the relative phases of Europa and Ganymede at the patch point. For simplicity, we select the U_1 surface in the Jupiter-Ganymede rotating frame to coincide with the U_1 surface in the Jupiter-Europa rotating frame at the patch point. Figure 14 shows the curves $^{\mathrm{Gan}}\gamma^1_{z\dot{z}}$ and $^{\mathrm{Eur}}\gamma^2_{z\dot{z}}$ on the $(x, \dot{x})$-plane in the Jupiter-Europa rotating frame for all orbits in the Poincaré section with points $(z, \dot{z})$ within $(0.0160 \pm 0.0008, \pm 0.0008)$. The size of this range is about 1000 km in z position and 20 m/s in z velocity.

From Figure 14, an intersection region on the $x\dot{x}$-projection is seen. We pick a point within this intersection region, but with two differing y velocities; one corresponding to $^{\mathrm{Gan}}W^u_+(\mathcal{M}^1)$, the tube of transit orbits coming from Ganymede, and the other corresponding to $^{\mathrm{Eur}}W^s_+(\mathcal{M}^2)$, the orbits heading toward Europa. The discrepancy between these two y velocities is the ΔV necessary for a propulsive maneuver to transfer between the two tubes of transit orbits, which exist at different energies.

18

Four-Body System Approximated by Coupled PCR3BP. In order to determine the transfer ΔV, we compute the transfer trajectory in the full 4-body system, taking into account the gravitational attraction of all three massive bodies on the spacecraft. We use the dynamical channel intersection region in the coupled 3-body model as an initial guess which we adjust finely to obtain a true 4-body bi-circular model trajectory.

Figure 4 is the final end-to-end trajectory. A ΔV of 1214 m/s is required at the location marked. We note that a traditional Hohmann (patched 2-body) transfer from Ganymede to Europa requires a ΔV of 2822 m/s. Our value is only 43% of the Hohmann value, which is a substantial savings of on-board fuel. The transfer flight time is about 25 days, well within conceivable mission constraints. This trajectory begins on a jovicentric orbit beyond Ganymede, performs one loop around Ganymede, achieving a close approach of 100 km above the moon's surface. After the transfer between the two moons, a final additional maneuver of 446 m/s is necessary to enter a high inclination (48.6°) circular orbit around Europa at an altitude of 100 km. Thus, the total ΔV for the trajectory is 1660 m/s, still substantially lower than the Hohmann transfer value.

Conclusion and Future Work.

In our current work on the spatial three-body problem, we have shown that the invariant manifold structures of the collinear libration points still act as the separatrices for two types of motion, those inside the invariant manifold "tubes" are transit orbits and those outside the "tubes" are non-transit orbits. We have also designed a numerical algorithm for constructing orbits with any prescribed finite itinerary in the spatial three-body planet-moon-spacecraft problem. As our example, we have shown how to construct a spacecraft orbit with the basic itinerary $(X; M, I)$ and it is straightforward to extend these techniques to more complicated itineraries.

Furthermore, we have applied the techniques developed in this paper towards the construction of a three dimensional Petit Grand Tour of the Jovian moon system. Fortunately, the delicate dynamics of the Jupiter-Europa-Ganymede-spacecraft 4-body problem are well approximated by considering it as two 3-body subproblems. One can seek intersections between the channels of transit orbits enclosed by the stable and unstable manifold tubes of the NHIM of different moons using the method of Poincaré sections. With maneuvers sizes (ΔV) much smaller than that necessary for Hohmann transfers, transfers between moons are possible. In addition, the three dimensional details of the encounter of each moon can be controlled. In our example, we designed a trajectory that ends in a high inclination orbit around Europa. In the future, we would like to explore the possibility of injecting into orbits of all inclinations.

References:

1. Howell, K., B. Barden and M. Lo, Application of Dynamical Systems Theory to Trajectory Design for a Libration Point Mission, *Journal of the Astronautical Sciences*, **45**, No. 2, April-June 1997, pp. 161-178.

2. Gómez, G., J. Masdemont and C. Simó, Study of the Transfer from the Earth to a Halo Orbit around the Equilibrium Point L_1, *Celestial Mechanics and Dynamical Astronomy* **56** (1993) 541–562 and **95** (1997), 117–134.

3. Koon, W.S., M.W. Lo, J.E. Marsden and S.D. Ross, The Genesis Trajectory and Hetero-clinic Connections, *AAS/AIAA Astrodynamics Specialist Conference*, Girdwood, Alaska, 1999, AAS99-451.

4. Koon, W.S., M.W. Lo, J.E. Marsden, and S.D. Ross, Heteroclinic Connections between Peri-odic Orbits and Resonance Transitions in Celestial Mechanics, *Chaos* **10**(2), 2000, 427–469.

5. Koon, W. S., M.W. Lo, J. E. Marsden and S.D. Ross [2001], Resonance and Capture of Jupiter Comets, *Celestial Mechanics and Dynamical Astronomy*, to appear

6. Koon, W.S., M.W. Lo, J.E. Marsden and S.D. Ross [2001], Low Energy Transfer to the Moon, *Celestial Mechanics and Dynamical Astronomy*, to appear.

7. Koon, W.S., M.W. Lo, J.E. Marsden and S.D. Ross [1999], Constructing a Low Energy Transfer between Jovian Moons, *Proceedings of the International Conference on Celestial Mechanics*, Northwestern University, Chicago, Illinois, 1999, to appear.

8. Abraham, R. and J.E. Marsden, *Foundations of Mechanics.* Second Edition, 1978, Addison-Wesley.

9. Marsden, J.E. and T.S. Ratiu, *Introduction to Mechanics and Symmetry.* Texts in Applied Mathematics, **17**, Springer-Verlag, 1994. Second Edition, 1999.

10. Szebehely, V.,*Theory of Orbits.* Academic Press, 1967, New York/London.

11. Conley, C.,Low Energy Transit Orbits in the Restricted Three-Body Problem. *SIAM J. Appl. Math.* **16**, 1968, 732–746.

12. McGehee, R. P., Some Homoclinic Orbits for the Restricted Three-Body Problem, *Ph.D. thesis*, 1969, University of Wisconsin.

13. Appleyard, D.F., Invariant Sets near the Collinear Lagrangian Points of the Nonlinear Re-stricted Three-Body Problem, *Ph.D. thesis*, 1970, University of Wisconsin.

14. Wiggins, S. [1994] *Normally Hyperbolic Invariant Manifolds in Dynamical Systems*, Springer-Verlag, New York.

15. Moser, J., On the Generalization of a Theorem of A. Liapunov, *Comm. Pure Appl. Math.*, XI, 1958, 257-271.

16. Hartman, P.,*Ordinary Differential Equations*, Wiley, New York, 1964.

17. Wiggins, S., L. Wiesenfeld, C. Jaffé and T. Uzer [2001] Impenetrable Barriers in Phase Space, *preprint.*

18. Gómez, G. and J. Masdemont, Some Zero Cost Transfers between Libration Point Orbits, AAS Paper 00-177, AAS/AIAA Astrodynamics Specialist Conference, Florida, 2000.

19. Jorba, À. and J. Masdemont, Dynamics in the Center Manifold of the Collinear Points of the Restricted Three Body Problem, *Physica D* **132**, 1999, 189-213.

20. Gómez, G., À. Jorba, J. Masdemont and C. Simó, *Dynamics and Mission Design near Libration Points, Vol III, Advanced Methods for Collinear Points*, World Scientific, 2001.